Applied Thermal Engineering 200 (2022) 117642

Contents lists available at ScienceDirect

Applied Thermal Engineering

journal homepage: www.elsevier.com/locate/ate

Research Paper

Parametric CFD study for finding the optimal tube arrangement of a fin-and-tube heat exchanger with plain fins in a marine environment

Turo Välikangas [a,*], Mikko Folkersma [b], Miikka Dal Maso [a], Tuomo Keskitalo [c], Petteri Peltonen [d], Ville Vuorinen [e]

[a] Aerosol Physics Laboratory, Physics Unit, Tampere University, Finland
[b] Faculty of Aerospace Engineering, Delft University of Technology, Netherlands
[c] Neste Engineering Solutions Oy, Finland
[d] Technical Research Centre of Finland, FI-02044 VTT, Finland
[e] Department of Mechanical Engineering, Aalto University, Finland

ARTICLE INFO

Keywords:
Fin-and-tube
Heat exchanger
Plain fin
Conjugate heat transfer

ABSTRACT

In the past, fin-and tube heat exchanger (FTHE) tube pattern ratios have been largely based on ad-hoc design principles. Here, we investigate the optimal tube arrangements for a FTHE with plain fins in marine environments represented by two different air types; one for unfiltered air with high condensation rate and one for clean dry filtered air conditions. The thermal-hydraulic efficiency of the FTHE design is measured by comparing a modified ratio of Colburn j-factor and Fanning friction factor. The regression model generated from the CFD data is then used to identify the maximum efficiency for two design specific fin pitches separately. We identified two optimal tube patterns: one for a large fin pitch for unfiltered air, and another for a small fin pitch for filtered air. Manufacturing restrictions were found to significantly limit the maximum achievable efficiency of a tube pattern. By neglecting the related manufacturing restrictions, 4% higher efficiency for a fin pitch of 1.5 mm and 23% higher efficiency for a fin pitch of 3.5 mm is achieved. Without any application specific limitations or manufacturing restrictions the fin pitch 1.5 mm can have a 36% increased efficiency than fin pitch 3.5 mm. These novel results show that development in manufacturing have potential for significant improvements in thermal-hydraulic efficiency.

1. Introduction

The heating ventilation and air conditioning (HVAC) system is the second largest energy consumer in a cruiser ship following the propulsion system [1]. The energy consumption of the HVAC system is highly dependent on the outside temperature, but in some estimates the energy consumption of the HVAC system can be up to 13%–16% [2,3]. Due to the COVID19 pandemic, it is possible that the use of fully separated fresh-exhaust air conditioning systems will increase in the future. Such designs can be achieved by using fin-and-tube heat exchanger (FTHE) -based heat recovery systems. In a FTHE-based heat recovery system the heat is transferred by a fluid in such a way that no mixing between fresh and exhaust air occurs. Unfortunately, this may lead to the overall decrease of efficiency in HVAC systems due to lack of recycled air. As the need for more efficient air conditioning units is evident, it is essential to improve the thermal-hydraulic efficiency of the heat exchanger inside the units.

The performance of the FTHE can be adjusted by changing the fin pitch [4], size of the tubes [5], longitudinal tube pitch [6], transverse tube pitch [7], number of tube rows [8], number of fluid circuits [9], the mass flow of the fluid [10] or the fin shape itself [11]. The challenge in comparing the performance of different fin shapes is the difficulty to reproduce the thermal-hydraulic efficiencies in a comparable manner. Experimental results of the performance of different fin types by multiple authors have been compiled into correlation studies [12–16]. In these, the results of multiple experimental studies are expressed in terms of correlation equations. This enables the fin designs to be intercompared in the whole design space with other variables that affect the thermal-hydraulic efficiency, such as fin pitch, tube diameter, tube pattern and fin thickness. Naturally, in the experimental studies, the authors are reporting values of real existing FTHE designs that are manufactured with applicable machinery. This means that data from uncommon combinations, which are rare in the industry, are absent. In

* Corresponding author.
E-mail addresses: turo.valikangas@tuni.fi (T. Välikangas), miikka.dalmaso@tuni.fi (M. Dal Maso), petteri.peltonen@vtt.fi (P. Peltonen), ville.vuorinen@aalto.fi (V. Vuorinen).

https://doi.org/10.1016/j.applthermaleng.2021.117642
Received 20 May 2021; Received in revised form 30 September 2021; Accepted 3 October 2021
Available online 22 October 2021

Nomenclature

Symbols

$\dot{m}$	Mass flow, kgs^{-1}
$\overline{h}$	Overall average heat transfer coefficient, $Wm^{-2}\ K^{-1}$
A	Wet area, m^2
$A_{freeflow}$	Free flow area, m^2
A_{front}	Front inlet area, m^2
C_f^p	Specific heat of the air, $Jkg^{-1}\ K^{-1}$
C_s	Specific heat of the fin, $Jkg^{-1}\ K^{-1}$
D	Tube diameter after expansion, m
D_h	Hydraulic diameter, based on free flow and wet area, m
D_c	Tube collar diameter, m
D_{in}	Tube inner diameter, m
f	Fanning friction factor
F_p	Fin pitch, m
G_k	Production term for k, $kgm^{-1}s^{-3}$
G_ω	Production term for ω, $kgm^{-3}s^{-2}$
j	Colburn j-factor
JF	JF performance ratio
k	Turbulence kinetic energy, m^2s^{-2}
L	Depth of the heat exchanger in flow direction, m
Nu	Nusselt number
P_d	Diagonal tube pitch, m
P_l	Longitudinal tube pitch, m
P_t	Transversal tube pitch, m
Pr	Prandtl number
Q	Overall transferred heat to the air, W
q	Heat flux, $Wm^{-2}s^{-1}$
Re_{D_c}	Reynolds number, based on hydraulic diameter D_c
Re_{D_h}	Reynolds number, based on hydraulic diameter D_h
T	Temperature, K
T_f	Temperature of the fluid, K
T_s	Temperature on the surface, K
T_w	Temperature at the wall, K
T_{inlet}	Temperature at the inlet, K
T_{lm}	Logarithmic mean temperature difference, K
T_{outlet}	Temperature at the outlet, K
u	Velocity in the direction of x axis, ms^{-1}
u_i	Velocity in the direction of each cartesian directions, ms^{-1}
u_{core}	Velocity in the minimum cross-sectional flow area, ms^{-1}
v	Velocity in the direction of y axis, ms^{-1}
w	Velocity in the direction of z axis, ms^{-1}
x_i	Cartesian coordinates x,y,z, m

Greek symbols

Δp	Pressure loss, Pa
η	Fin efficiency
Γ	Turbulent viscosity, $kgm^{-1}s^{-1}$
κ	Air thermal diffusivity, $Wm^{-1}s^{-1}$
λ_f	Thermal conductivity of the air, $Wm^{-1}K^{-1}$
λ_s	Thermal conductivity of the fin, $Wm^{-1}K^{-1}$
μ	Dynamic viscosity of air, $kgm^{-1}s^{-1}$
ν	Kinematic viscosity of the air, m^2s^{-1}
ω	Turbulence specific dissipation, s^{-1}
ρ	Density of the air, kgm^{-3}
θ	Non-dimensionalized temperature

Subscripts

f	Fluid
i, j, k	Cartesian coordinate directions, -
s	Solid

Superscripts

p	Constant pressure

addition to this, not all possible combinations have been measured and therefore the real relation between the fin shape and design parameters and their effect on the thermal-hydraulic efficiency is obscured. In other words, the variables used in the designs are not selected evenly to cover all parts of the design space in an equal and unbiased manner. Therefore, such literature data may be biased towards certain designs.

Ameel et al. [17] showed that a lighter and smaller FTHE can be made with a smaller fin pitch. However, there is often an application specific threshold that enforces the use of a wider fin spacing. Therefore, in cooling coils with high condensation rates, often only plain fin types with relatively high fin pitches are used. Such occasions are for example hygiene-related applications that are used in hospital environments. Other examples include applications with higher amounts of condensate rate [18], hazardous air with increased fouling propensity [19] or the risk of ice formation [20] on the fins. Hence, the tube arrangement needs to be specifically optimized for each application-specific fin spacing and inlet velocity. Therefore, as noted in the present study, it may be important for the manufacturer of the FTHE to know which tube arrangements are the best for a given application.

As mentioned earlier, in experimental FTHE studies the designs are very often biased towards the pre-existing portfolio that is being manufactured already in the industry. In contrast, in CFD-based FTHE studies the manufacturing restrictions or difficulties are often neglected. For example, a very common rule that is followed in the industry is to use a tube pattern that has the ratio of traversal tube pitch to longitudinal tube pitch $P_t/P_l = 1.1547$. This enables the manufacturer to use only one kind of U-bend tubes in the process of soldering the circuits. Experimental studies found in the literature on the thermal-hydraulic efficiency of FTHE with plain fins [13,14,21–25] have a 61% portion with the aforementioned ratio. Another popular tube arrangement ratio was $P_t/P_l = 1.333$ with 24% of all the designs. We do not have an explanation for the use of the latter ratio but the first one is further analyzed in Section 4 where its effect on the thermal-hydraulic efficiency is illustrated.

Based on the literature, previous dimensional characterizations of FTHE's have been done mostly on ad-hoc principles following traditional guidelines. Here, we make an attempt to systematically assess such FTHE design by CFD, utilizing a novel open source meshing tool called Swiftblock along with the open source CFD library OpenFOAM. The main objectives of this study are as follows: 1) Develop a parametric computational conjugate heat transfer model to explore different fin spacings and tube arrangements. 2) Carry out a systematic parameter sweep for transverse ($P_t = 14–38$ mm) and longitudinal ($P_l = 14–78$ mm) tube distances. Repeat the parametric sweep for two

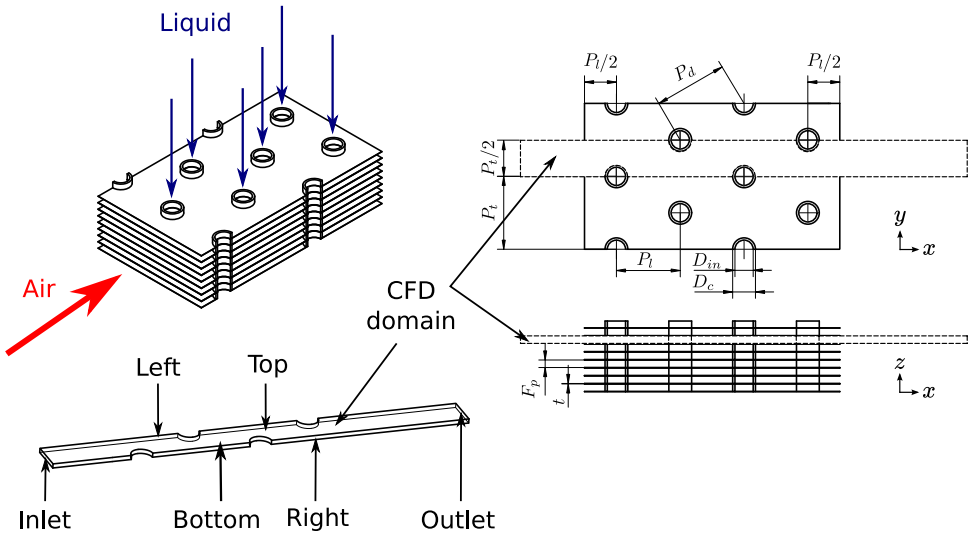

Fig. 1. Illustration of the simulated geometry between the fins and tubes of the fin-and-tube heat exchanger. The main parameters studied herein are P_l and P_t for two different fin pitches F_p.

different fin pitch values. A typical marine application design point with the velocity of $u = 3\,\mathrm{m\,s^{-1}}$ was chosen for the inlet boundary condition. Other variables such as number of tube rows $N = 4$, tube diameter $D_c = 10.00\,\mathrm{mm}$ and the fin thickness $t = 0.2\,\mathrm{mm}$ are kept constant. 3) Create a regression model based on performance ratio data. 4) Find the optimal tube pattern value from the model when the manufacturing restrictions have to be followed and when they can be arbitrarily selected based on the goodness of the design.

This study offers a novel approach for creating the computational model with automatic open source meshing, so that larger parametric design spaces can be studied. The study offers a valuable data set outside the previously investigated ranges available in the literature. The published data set can be used to find optimal solutions for various FTHE designs. Additionally, this study illustrates that for maximizing the JF performance ratio, the best design is not found within the current design portfolio broadly used in the industry.

2. Details on the numerical domain and performance parameters

2.1. Plain fin-and-tube heat exchanger simulation domain

The computational domain is designed in a way that it represents the characteristics of the air side heat transfer in any size of heat exchanger inlet area but requires a feasible amount of computational resources. It is expected that by multiplying this to match the face area of arbitrary sized heat exchanger, the air side heat transfer rate scales equally. Therefore, only one flow section between the tubes and the fins is simulated. In Fig. 1 is an illustration of the FTHE and the computational domain that is modeled.

Before and after the heat exchanger we model an inflow and an outflow region with the length of one and two longitudinal tube pitches, respectively.

2.2. Data reduction and performance parameters

In this study, the Reynolds number is defined in two different ways. The first one in Eq. (1) is based on the hydraulic diameter $D_h = \frac{4A_{free\,flow}L}{A}$ [26] as the reference length scale and the used reference velocity is the average velocity in the minimum cross section called the core velocity u_{core}.

$$Re_{D_h} = \frac{u_{core} D_h}{\nu} \tag{1}$$

The second is used when the CFD values are compared to the experimental results in Section 3.3 and is therefore defined as:

$$Re_{D_c} = \frac{u_{core} D_c}{\nu} \tag{2}$$

where $D_c = 10.00\,\mathrm{mm}$ is the collar tube diameter, which can be calculated as $D_c = D + 2 * t$. The overall average heat transfer coefficient in the case of a FTHE is calculated as:

$$\overline{h} = \frac{Q}{A \Delta T_{lm}} \tag{3}$$

where $Q = \dot{m} C_f^p (T_{inlet} - T_{outlet})$ is the overall transferred heat to the air and ΔT_{lm} is the logarithmic mean temperature difference between the inside diameter of the tube and the air.

The results in this study are illustrated in the form of a non-dimensional pressure drop, the Fanning friction factor f [27,28], and the non-dimensional heat transfer, Colburn j-factor [29], which are calculated as follows.

$$j = \frac{Nu}{Re_{D_h} Pr^{1/3}} = \frac{\frac{\overline{h} D_h}{\lambda_f}}{\frac{\rho u_{core} D_h}{\mu}} Pr^{2/3} \tag{4}$$

$$f = \frac{\Delta p}{\frac{1}{2}\rho u_{core}^2} \times \frac{D_h}{4L} \tag{5}$$

In general, increase in heat transfer yields an increase in pressure drop. This means that one must consider the trade-off between the increase in heat transfer and increase on the pressure drop when evaluating the performance of the heat exchanger. Traditionally the performance of the fin shapes are compared with goodness factors such as area [30,31] or volume goodness [30,32,33]. However, using these presents some difficulties when the reference length and/or velocity scales are different between the cases [34]. In this study, all the reference variables change between the cases. Therefore, it is desirable to use a performance criterion that has a numerical value that increases with improved performance, regardless of reference scales. One such performance criterion is the JF performance rate, as defined by Shi et al. [35] and Yun and Lee [36] (see references for the derivation). We apply a version of the JF performance ratio in which the reference variables are not subtracted from the equation. JF is defined as the ratio of two other important ratios obtained between a studied heat exchanger and a reference heat exchanger. One is the ratio of the heat transfer rate per unit temperature difference, per unit surface area, and

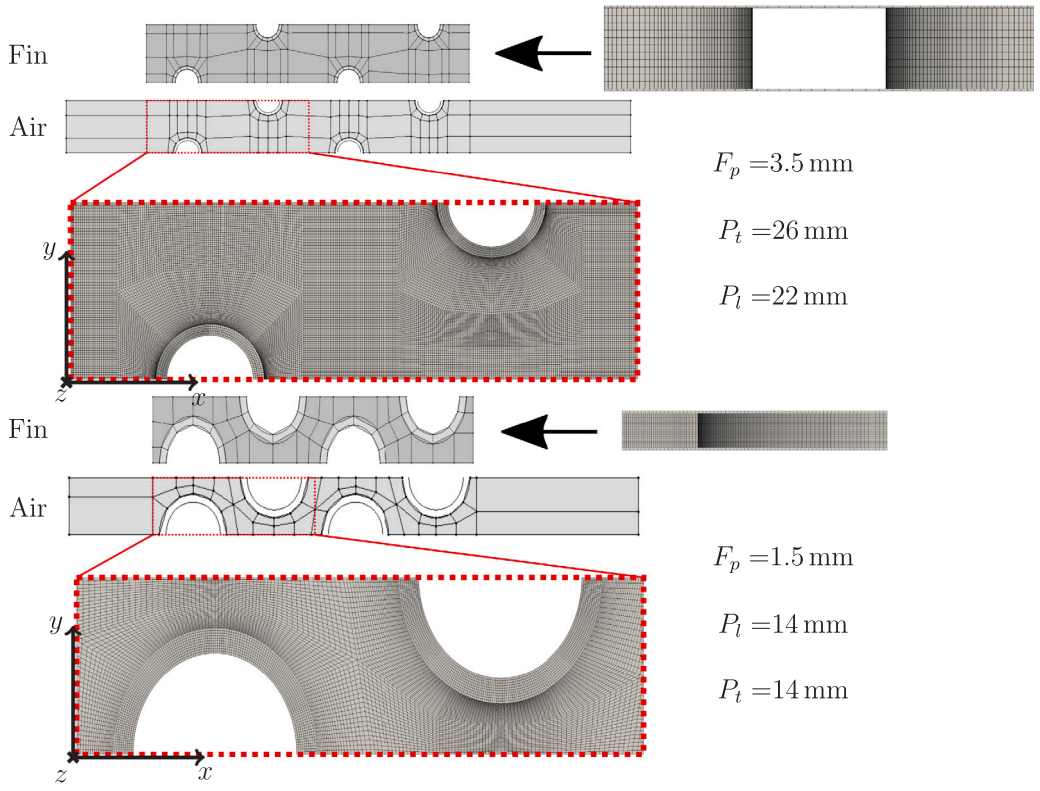

Fig. 2. Illustration of the two different blocking strategies used for the fin and air mesh.

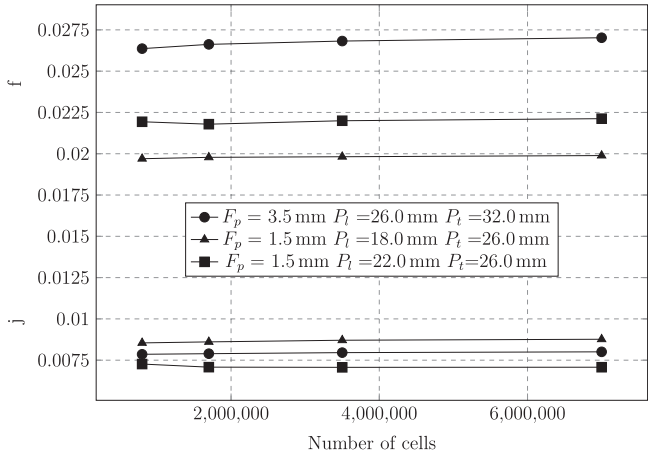

Fig. 3. Mesh sensitivity of the non-dimensional pressure drop (Fanning friction factor f) and heat transfer (Colburn j-factor j). Overall root mean square percentage error respect to the finest grid was 1.97% for 800k mesh, 1.4% for 1.7 million cell mesh and 0.79% for the 3.5 million cell mesh.

the other is the ratio of the friction power dissipated per unit surface area.

The ratio of the heat transfer rate per unit temperature, per unit area of studied heat exchanger and reference heat exchanger is shown in Eq. (6).

$$\frac{\overline{h}}{\overline{h}_R} = \frac{j}{j_R} \times \frac{(Re_{D_h}/D_h)}{(Re_{D_h}/D_h)_R} \tag{6}$$

The ratio of the friction power dissipated per unit area of studied heat exchanger and reference heat exchanger is shown in Eq. (7).

$$\frac{(P/A)}{(P/A)_R} = \frac{f}{f_R} \times \frac{(Re_{D_h}/D_h)^3}{(Re_{D_h}/D_h)^3_R} \times \frac{A_{front}}{A_{frontR}} \times \frac{A_R}{A} \tag{7}$$

Therefore, we define the JF performance ratio as

$$JF = \frac{\frac{\overline{h}}{\overline{h}_R}}{(\frac{(P/A)}{(P/A)_R})^{1/3}} = \frac{\frac{j}{j_R} \times \frac{(Re_{D_h}/D_h)}{(Re_{D_h}/D_h)_R}}{(\frac{f}{f_R} \times \frac{(Re_{D_h}/D_h)^3}{(Re_{D_h}/D_h)^3_R} \times \frac{A_{front}}{A_{frontR}} \times \frac{A_R}{A})^{1/3}} \tag{8}$$

where the A_{front} is the inlet area of the flow domain and A is the heat transfer area of the FTHE. The subscript R refers to the reference design, which is chosen as the one with P_l = 14 mm, P_t = 14 mm and F_p = 1.5 mm.

2.3. Governing equations and boundary conditions

The equations describe a steady-state, incompressible, three-dimensional flow with no sink or source terms. The governing equations that describe the conjugate heat transfer process in the fin-and-tube heat exchanger are the continuity equation in Eq. (9), momentum equation in Eq. (10) and the energy equation for fluid in Eq. (11) as well as for solid regions in Eq. (14). Turbulence is modeled with the $k-\omega$ Shear-Stress Transport (SST) model, which considers the enhanced wall treatment as default and is widely used in FTHE simulations [37–39]. The transport equation for turbulence kinetic energy is shown in Eq. (12) and for the specific turbulence dissipation rate in Eq. (13).

1. Continuity equation

$$\frac{\partial(\rho u_i)}{\partial x_i} = 0 \tag{9}$$

2. Momentum equation

$$\frac{\partial}{\partial x_i}(\rho u_i u_j) = \frac{\partial}{\partial x_i}(\mu \frac{\partial u_j}{\partial x_i}) - \frac{\partial p}{\partial x_j} \tag{10}$$

3. Energy equation for fluid region

$$\frac{\partial}{\partial x_i}(\rho C_f^p u_i T) = \frac{\partial}{\partial x_i}(\lambda_f \frac{\partial T}{\partial x_i}) \tag{11}$$

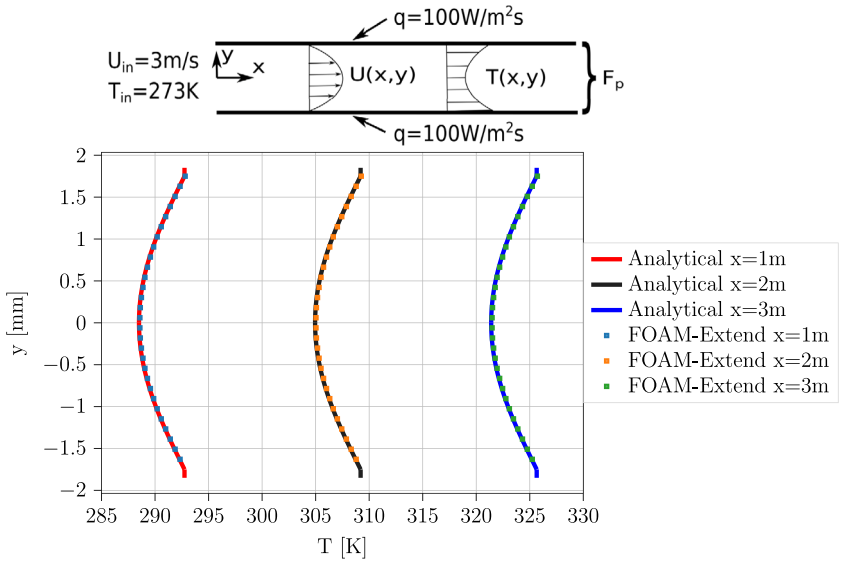

Fig. 4. Temperature profile comparison between the analytic and CFD results for laminar channel flow with conjugate heat transfer in a 2D channel flow with constant heat flux for which an analytic solution exists.

Table 1
Boundary conditions used for the computational model.

Boundary name	Boundary condition
Inlet	$u = constant, v = w = 0, T = 273$ K
Outlet	$\frac{\partial u_i}{\partial x} = \frac{\partial T}{\partial x} = 0$
Inflow and outflow regions	
Top and bottom	$\frac{\partial u}{\partial z} = \frac{\partial v}{\partial z}, w = 0, \frac{\partial T}{\partial z} = 0$
Left and right	$\frac{\partial u}{\partial y} = \frac{\partial v}{\partial y}, v = 0, \frac{\partial T}{\partial y} = 0$
Fin region	
Top and bottom	$\frac{\partial u}{\partial z} = \frac{\partial v}{\partial z}, w = 0, \frac{\partial T}{\partial z} = 0$
Left and right	Tube inner surface $u = v = w = 0$, $T = 333$ K Fin region $u = v = w = 0$, $\frac{\partial T}{\partial y} = 0$ Fluid region $\frac{\partial u}{\partial y} = \frac{\partial w}{\partial y}, \frac{\partial T}{\partial y} = 0$
Fluid–solid interface	$T_s = T_f, -\lambda_s \frac{\partial T_s}{\partial n} = -\lambda \frac{\partial T_f}{\partial n}$

4. Transport equation for the turbulence kinetic energy, k

$$\frac{\partial}{\partial x_i}(\rho k u_i) = \frac{\partial}{\partial x_j}(\Gamma_k \frac{\partial k}{\partial x_j}) + G_k \tag{12}$$

5. Transport equation for the specific turbulence dissipation rate, ω

$$\frac{\partial}{\partial x_i}(\rho \omega u_i) = \frac{\partial}{\partial x_j}(\Gamma_\omega \frac{\partial \omega}{\partial x_j}) + G_\omega \tag{13}$$

6. Energy equation for solid region

$$\frac{\partial}{\partial x_i}(\lambda_s \frac{\partial T}{\partial x_i}) = 0 \tag{14}$$

The boundary conditions used in the computational domain are defined in Table 1. Please see the locations of inlet, outlet, top, bottom, left and right boundaries in Fig. 1.

The governing equations are solved with a solver called conjugateHeatSimpleFoam from the foam-extend 4.0 [40] a community driven version of the OpenFOAM library.

3. Meshing and model validation

3.1. Parametric structured meshing

Altogether 198 simulations are carried out by varying the fin pitch and tube pattern inside the FTHE. In a parametric FTHE study, where

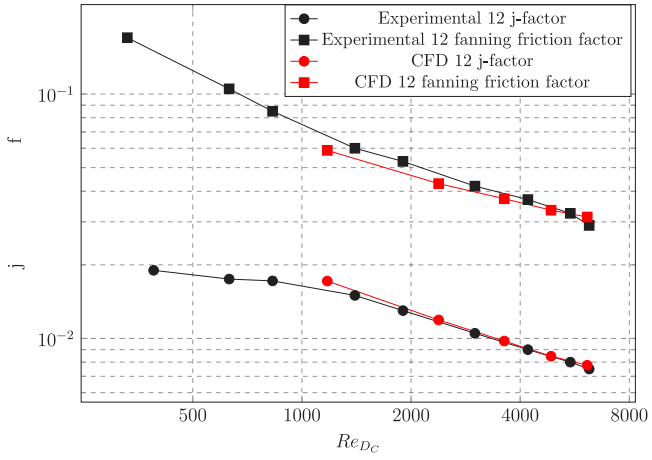

Fig. 5. Model validation by comparing the results of CFD pressure drop and heat transfer to the experimental results by Wang et al. [27].

only a few of the parameters are changed at once and rest of the design stays the same, parametric structured meshing can be superior over unstructured meshing strategies. For this purpose, a novel parametric open source meshing tool Swiftblock developed by the authors (https://swiftblock.readthedocs.io/) was used. The authors have successfully used the meshing tool in multiple different studies in the past [41–43]. The blocking strategies that were created for the plain fin FTHE are illustrated in Fig. 2. The lower two blockings for fin and air are used for cases with P_l = 14.00–22.00 mm in conjunction with P_t = 14.00–20.00 mm. The upper two figures are used for the rest of the designs.

3.2. Mesh sensitivity

As no wall function were used in the simulations, a fine mesh was used at the wall to assure accurately resolved boundary layer on the heat transfer surfaces. A y-value that translates to the average y^+-value of 0.25 was chosen with the maximum of around $y^+ = 2$ in the whole domain. Then a mesh sensitivity analysis was performed by changing the maximum cell size and keeping the y-value constant at the wall.

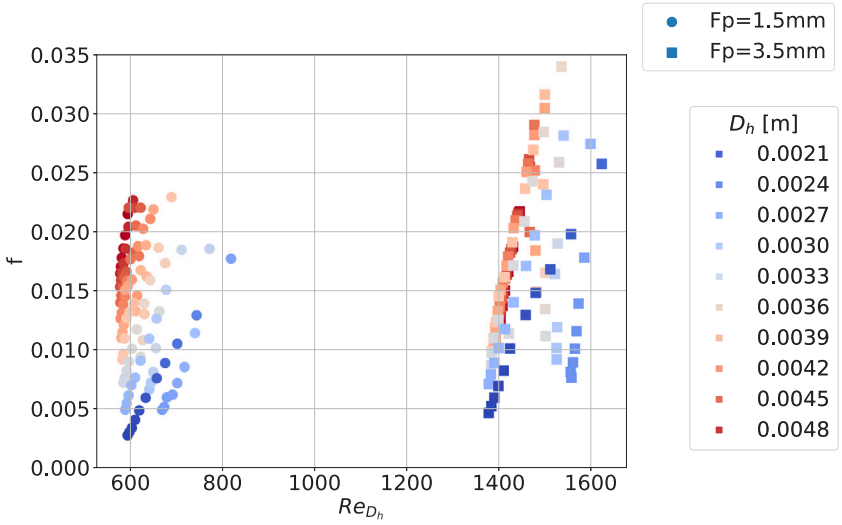

Fig. 6. Fanning friction factor observed in the present 198 simulated data points. The left cluster corresponds to the smaller fin pitch $F_p = 1.5\,\text{mm}$ while the right cluster corresponds to the larger pitch value $F_p = 3.5\,\text{mm}$. No clear difference in pressure drop can be seen between the fin pitches.

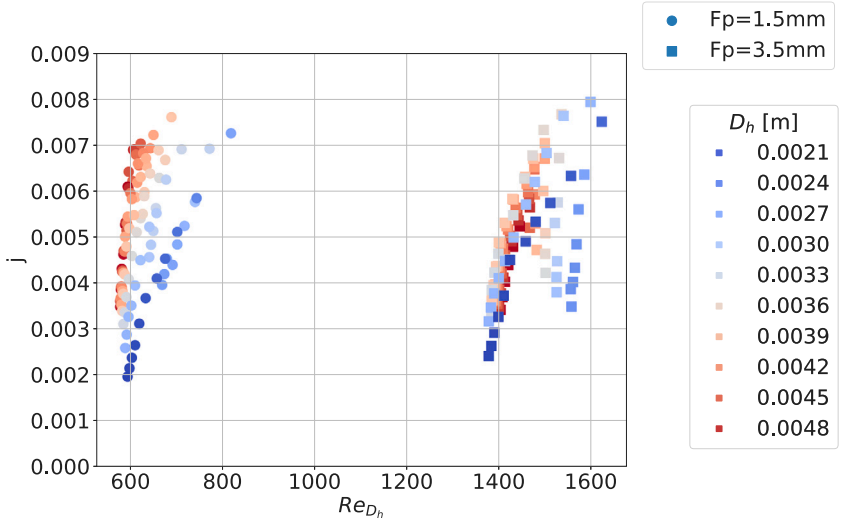

Fig. 7. Colburn j-factors observed in the present 198 simulated data points. Left cluster for smaller fin pitch $F_p = 1.5\,\text{mm}$ and right cluster for larger $F_p = 3.5\,\text{mm}$. No clear difference in heat transfer can be seen between the fin pitches.

The results are shown in Fig. 3 for pressure drop and heat transfer over the heat exchanger with the studied design variables.

Overall root mean square percentage error respect to the finest grid was 1.97% for 800 k mesh, 1.4% for 1.7 million cell mesh and 0.79% for the 3.5 million cell mesh. For a feasible trade off between computational resources and accuracy, first the data simulations for the surrogate models are made with 1.7 million cell mesh and then the maximum values are simulated with the 3.5 million cell size mesh.

3.3. Solver verification and model validation

In Fig. 4, the solver was verified by comparing the CFD results computed with foam-extend to the analytical results for conjugate heat transfer of laminar channel flow with constant heat flux boundary condition illustrated in Eq. (15) for air and for solid in Eq. (16). [44,45]

$$T_f(x,y) = T_{mi} - \frac{3q}{\kappa F_p}\left(\frac{y^4}{3F_p^2} - \frac{y^2}{2} + \frac{5F_p^2}{48}\right) + \frac{17}{70}\frac{F_p q}{\kappa} + \frac{qP}{\dot{m}C_f^p}x \tag{15}$$

$$T_s(x,y) = T_w + \frac{q}{\lambda_s}y \tag{16}$$

All the material properties used for the solver validation in this study are identical to the ones tabulated in Appendix in Table 2 and the used fin pitch was $F_p = 3.5\,\text{mm}$ and fin thickness $t = 0.2\,\text{mm}$.

In Fig. 5, the computational model is validated by comparing the results over the heat exchanger to the experimental values created by Wang et al. [27]. The compared design was the number 12 in the study with $D_c = 10.23\,\text{mm}$, $t = 0.2\,\text{mm}$, $F_p = 1.77\,\text{mm}$, $P_t = 25.4\,\text{mm}$ and $P_l = 22.0\,\text{mm}$. As opposed to all other calculations in this study, for the model validation, the fin efficiency $\eta = 0.93 - 0.85$ was excluded from the heat transfer coefficient calculation to be consistent with the experimental results [27]. All other parameters and numerical details were chosen to be identical with the ones used in this study.

Acceptable agreement was seen between the CFD and the experimental results with the root mean square error of 0.00067 (5.0%) for j-factor and 0.003 (6.4%) for friction factor. Therefore, a conclusion is made that the model can be used for the analysis of thermal-hydraulic efficiency of the FTHE.

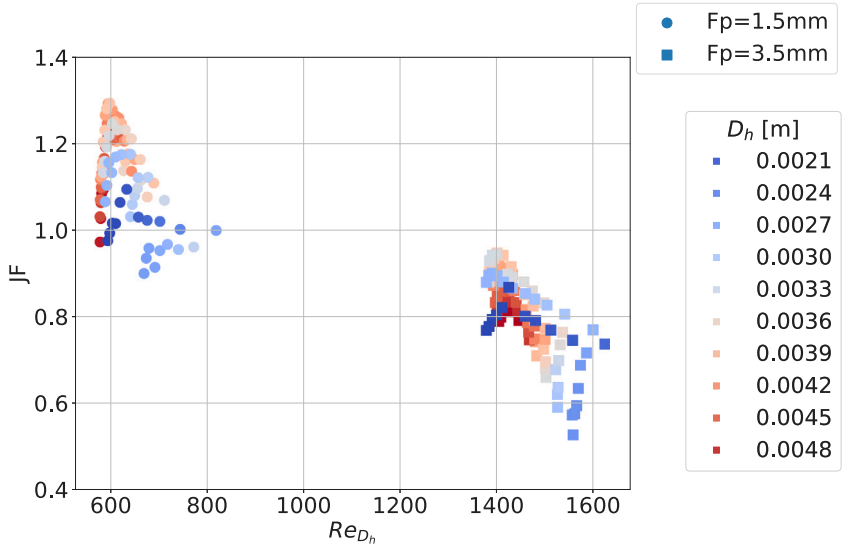

Fig. 8. JF performance ratio respect to the Reynolds number observed in the present 198 simulated data points. Left cluster represents a smaller fin pitch $F_p = 1.5\,\text{mm}$ while the right cluster the larger value $F_p = 3.5\,\text{mm}$. Left cluster clearly outperforms the right cluster in terms of the JF performance ratio.

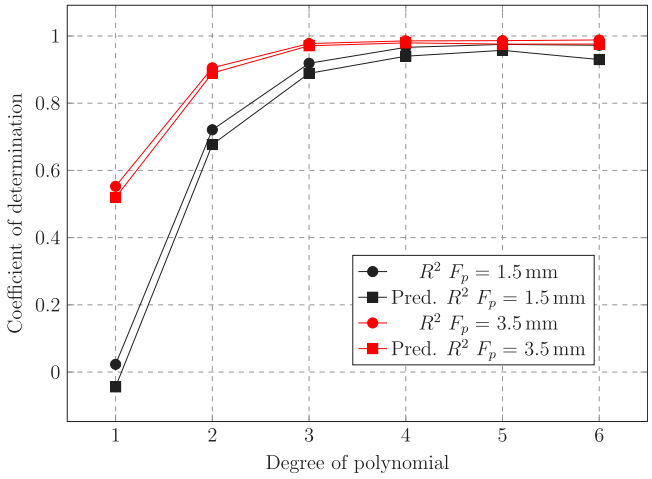

Fig. 9. Coefficient of determination R^2 and predictive R^2 with different degrees of polynomial regression models.

4. Results and discussion

4.1. Thermal-hydraulic performance of the simulated designs

In order to understand the thermal and hydraulic features of the different designs simulated in this study, all the CFD-results are first plotted as a function of the Reynolds number and colored with the hydraulic length scale $D_h = \frac{4A_{freeflow}L}{A}$. Traditionally this is the standard approach for investigating the characteristics of different FTHE designs. In fact, FTHE correlation equations are commonly based on Re_{D_h}, D_h and other physical parameters. The Fanning friction factor for all the simulated cases at different Reynolds numbers is shown in Fig. 6 (see Eq. (5)).

In Fig. 6, it is noted that friction factor values with the larger fin pitch seem to span a larger area than with the smaller fin pitch. When the coloring of the values is investigated in more detail, it can be seen that the larger hydraulic length scale values tend to accumulate in the north-east of the stack where as smaller hydraulic length scale values are seen on the south-west side of the stack. This observation applies to the bigger fin pitch as well but with a few outliers in the data. Due to the different length scales and reference velocities in each design, no clear correlation between the friction factor, Reynolds number and hydraulic length scale can be observed. The non-dimensional heat transfer parameter, the Colburn j-factor (see Eq. (4)), calculated for all cases is shown in Fig. 7 and the data points are again colored with the hydraulic length scale. Similar to the above, no clear correlation between j-factor and Reynolds number can be observed.

In order to see if the best performing tube pattern correlates with the Reynolds number or the hydraulic length scale, the JF performance ratio of the plain fin shape with all the different tube arrangement combinations calculated in this study are shown in Fig. 8. The left cluster with the smaller fin pitch $F_p = 1.5\,\text{mm}$ can be seen to clearly outperform the right cluster with the larger fin pitch $F_p = 3.5\,\text{mm}$. In other words, the larger the distance between the planar fins, and therefore larger heat transfer area, the worse the JF performance indicator for majority of the studied data points.

No similar trend can be found with the JF performance ratio and hydraulic length scale as was seen with j-factor and friction factor. As it was seen, there was no big difference between the thermal-hydraulic characteristics of the two different fin pitches, the difference in the JF performance ratio has to originate from geometric dimensions such as the inlet area and heat transfer area of the designs. Evidently, it is challenging to draw any direct conclusions on the relationship between the Reynolds number, the hydraulic length scale and the JF ratio in terms of the thermal-hydraulic performance of the different tube patterns in each fin pitch. For this reason, next a regression model is fitted on the data and visualized as a function of P_l and P_t separately for both fin pitches.

4.2. Regression model

Next, we aim at finding a polynomial regression to the data points. The benefit of such a regression model would be to find maximal JF performance ratio for a FTHE design. The regression polynomial is illustrated in Eq. (17):

$$\begin{aligned} y = {} & b_0 + b_1 P_l + b_2 P_t + b_{11} P_l^2 + b_{12} P_l P_t + b_{22} P_t^2 + b_{111} P_l^3 + b_{112} P_l^2 P_t \\ & + b_{122} P_l P_t^2 + b_{222} P_l^3 + b_{1111} P_l^4 + b_{1112} P_l^3 P_t + b_{1122} P_l^2 P_t^2 \\ & + b_{1222} P_l P_t^3 + b_{2222} P_t^4 \end{aligned} \tag{17}$$

where y is the response and b_1, b_{ii}, b_{iii}, b_{iiii}, b_{ij}, b_{iij}, b_{ijj}, b_{iiij}, b_{iijj} and b_{ijjj} are the linear regression coefficients. The quality of the

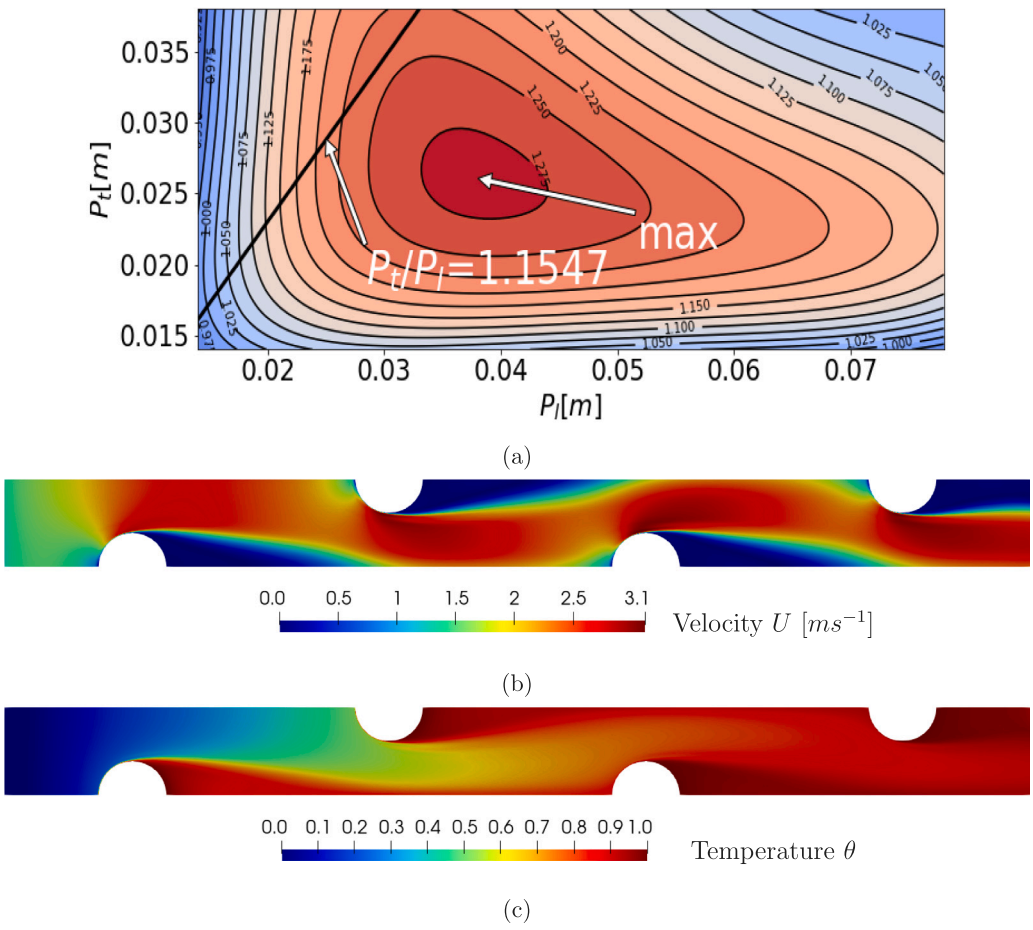

Fig. 10. (a) JF performance criteria response surface for F_p = 1.5 mm. The P_t/P_l = 1.1547 tube pattern ratio is illustrated with a black line. (b) Velocity in the middle of the channel in the design with F_p = 1.5 mm, P_l = 38.04 mm and P_t = 26.05 mm (c) Temperature in the middle of the channel in the design with F_p = 1.5 mm, P_l = 38.04 mm and P_t = 26.05 mm.

mathematical models is measured with the coefficient of determination R^2 which is the proportion of the variance in the dependent variable that is predictable from the independent variables. It is defined as

$$R^2 = 1 - \frac{SS_{res}}{SS_{tot}} \tag{18}$$

where $SS_{tot} = \sum_{n=i}(y_i - \bar{y})^2$ is the total sum of squares which is proportional to overall variance of the data and $SS_{res} = \sum_{n=i}(y_i - f_i)^2$ is the residual sum of squares. In regression, the R^2 coefficient of determination is a statistical measure of how well the regression predictions approximate the real data points. An R^2 of 1 indicates that the regression predictions perfectly fit the data. The predictive R^2 is calculated by removing each experiment separately, calculating the regression coefficients again and determining how well the model predicts the removed observation. The values of R^2 and predictive R^2 with different degrees of polynomial regression models can be seen in Fig. 9.

The 4th degree polynomial regression model was chosen and the coefficients of the model can be seen in Appendix in Table 3.

4.3. Results and discussions

The regression models are then used to visualize and locate the maximum value for the JF performance ratio for each fin pitch separately. In the present study, a sequential least squares quadratic programming (SLSQP) algorithm is used [46] to locate the maximum. SLSQP is an iterative method for constrained nonlinear optimization. In Fig. 10(a), the JF performance ratio for F_p = 1.5 mm can be seen to reach its maximum value of JF = 1.28 (j = 0.0061 , f = 0.0176). This corresponds to the longitudinal tube pitch of P_l = 38.04 mm ($3.8D_c$, $25.4F_p^{1.5\ \mathrm{mm}}$) and the traversal tube pitch of P_t = 26.05 mm ($2.6D_c$, $17.4F_p^{1.5\ \mathrm{mm}}$). The velocity and temperature fields of this design at the maximum JF performance ratio are then illustrated in Figs. 10(b) and 10(c). The temperature is non-dimensionalized according to the Eq. (19).

$$\theta = \frac{T - T_{inlet}}{T_w - T_{inlet}} \tag{19}$$

In Fig. 11(a), the JF performance ratio surface for F_p = 3.5 mm can be seen within the studied design space with the maximum value of JF = 0.94 (j = 0.0046 , f = 0.0129). This corresponds to the longitudinal tube pitch of P_l = 55.77 mm ($5.6D_c$, $15.9F_p^{3.5\ \mathrm{mm}}$) and the traversal tube pitch of P_t = 21.56 mm ($2.16D_c$, $6.16F_p^{3.5\ \mathrm{mm}}$). The velocity and temperature fields of this design in the middle of the channel are then illustrated in Figs. 11(b) and 11(c).

It can be seen that the design with the maximum JF performance ratio for the larger fin pitch has a larger longitudinal tube distance than with the one with the smaller fin pitch. On the contrary the best performing smaller fin pitch design has a larger transversal tube distance compared to the larger fin pitch. The best performing design in Figs. 10(b) and 10(c) with the smaller fin pitch has a relatively smooth velocity field with no clearly visible secondary flows that could enhance the heat transfer process. But in contrast, in the best performing design with larger fin pitch in Figs. 11(b) and 11(c), there is clearly two separate flow patterns that most likely increase the rate of heat transfer. In both design, the recirculation zone behind the tubes reaches the same level with the next tube row. It was already discussed that a smaller fin

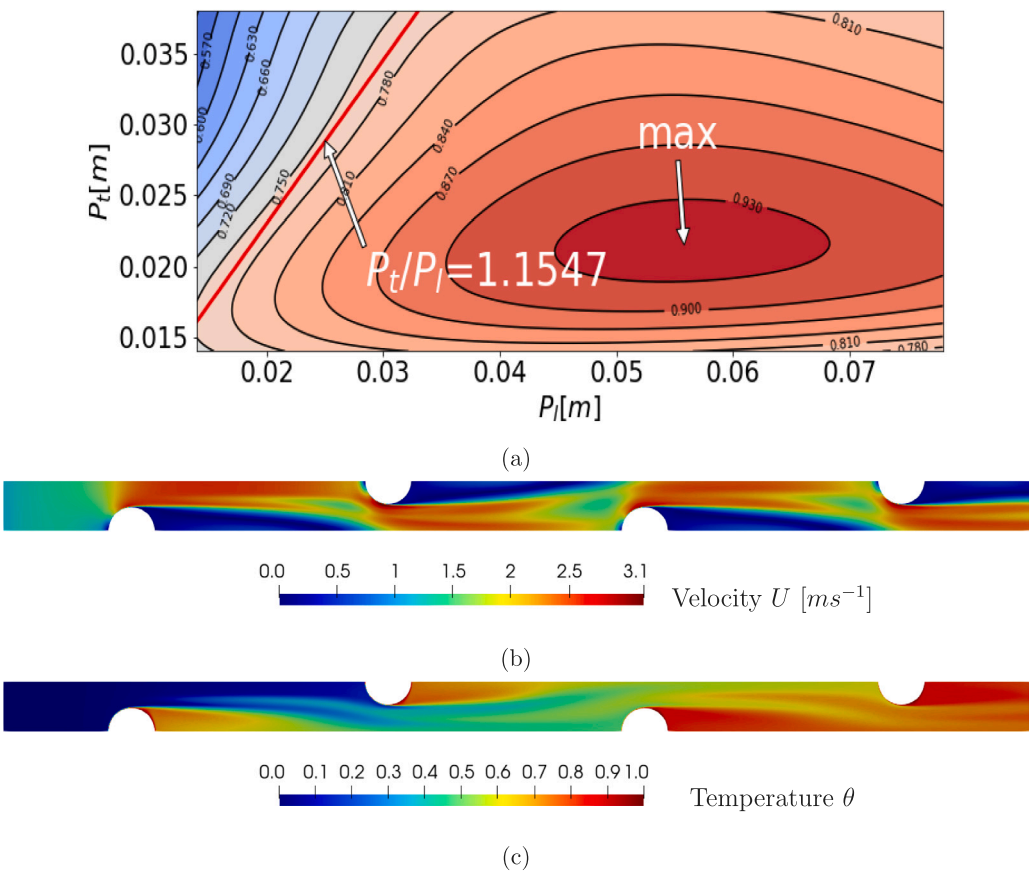

Fig. 11. (a) JF performance ratio response surface for F_p = 3.5 mm. The P_t/P_l = 1.1547 tube pattern ratio is illustrated with a red line. (b) Velocity in the middle of the channel in the design with F_p = 3.5 mm, P_l = 55.77 mm and P_t = 21.56 mm c) Temperature in the middle of the channel in the design with F_p = 3.5 mm, P_l = 55.77 mm and P_t = 21.56 mm.

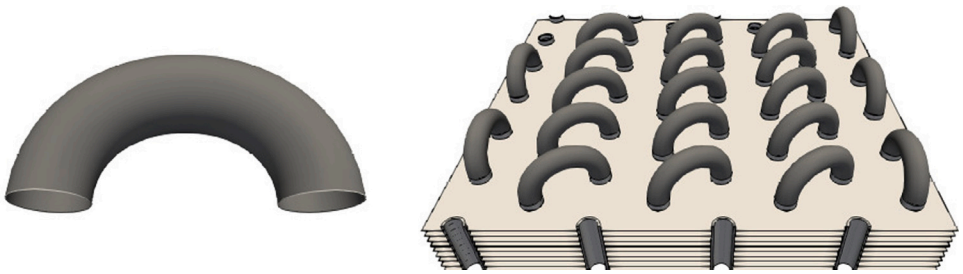

Fig. 12. Illustration of a one size U-bend in a situation where the $P_d = P_t$, therefore the same U-bend can be used to connect tubes vertically as well as tube rows horizontally to each other.

pitch enables lighter and smaller heat exchangers to be made [17]. In this study, the tube pattern with the highest performance ratio with the fin pitch of F_p = 1.5 mm can have a 36% higher JF performance ratio than the best performing tube pattern with fin pitch of F_p = 3.5 mm. This observation has a 32.6% higher j-factor and 36.4% higher friction factor.

In Figs. 10(a) and 11(a), the black and red line represents a manufacturing restriction that is widely followed in the industry. By using tube patterns that corresponds to the ratio of P_t/P_l = 1.1547, the transversal tube distance equals to the diagonal distance of the tube rows $P_t = P_d$ and therefore only one kind of U-bends can be used in the soldering process of the tube circuits. This means that the same U-bend can be used to connect tubes vertically as well as tube rows horizontally to each other as shown in Fig. 12. The values on along the line that follows the ratio of P_t/P_l = 1.1547 in two dimensional space can be found in Fig. 13.

If the FTHE is designed for an application with dry filtered air a smaller fin pitch of F_p = 1.5 mm can be used. Therefore, when the manufacturing restrictions related to the radius of the U-bends are neglected (i.e. the ratio P_t/P_l = 1.1547 is not enforced), a design with a 4% higher JF performance ratio can be achieved. The observation has a 7.6% lower j-factor and 6.0% higher friction factor. In an application with a high condensation rate, requiring a larger fin pitch of F_p = 3.5 mm, a 23% higher JF performance ratio can be achieved when deviating from the P_t/P_l = 1.1547 ratio. The unrestricted design has a 34.3% lower j-factor and 49% lower friction factor than the restricted design. The final decision of following the tube pattern ratio rule has to be made based on the extra cost related to manufacturing of two

Table 2
Thermophysical properties.

Property name	Variable	Value	Units
Fin thermal conductivity	λ_s	220	W m^{-1} K^{-1}
Air density	ρ_a	1.15	kg m^{-3}
Air Prandtl number	Pr	0.72	–
Air kinematic viscosity	ν	1.6e−5	m^{2}s^{-1}
Air heat capacity	C_f^p	1007	kg m^2 s^{-2} K^{-1}
Air thermal diffusivity	$\kappa = \rho_a C_f^p \nu / Pr$	0.025734	W m^{-1} K^{-1}

different U-bend sizes and the benefit gained by higher JF performance ratio of such heat exchangers.

With the wider fin pitch of $F_p = 3.5$ mm, there seems to be only a small difference between different tube patterns. The local maximum was seen to be $JF = 0.77$ ($j = 0.0070$, $f = 0.0253$) with $P_l = 17.58$ mm ($1.76D_c$, $5.02F_p^{3.5\ \mathrm{mm}}$) and $P_t = 20.22$ mm ($2.02D_c$, $5.78F_p^{3.5\ \mathrm{mm}}$). With the smaller fin pitch of $F_p = 1.5$ mm, there is a clear local maximum to be found at $P_l = 29.79$ mm ($2.98D_c$, $19.86F_p^{1.5\ \mathrm{mm}}$) and $P_t = 34.26$ mm ($3.43D_c$, $22.84F_p^{1.5\ \mathrm{mm}}$) with the value of JF =1.24 ($j = 0.0066$, $f = 0.0166$). Illustration of both these designs are shown in Fig. 14.

The best performing design that follows $P_t/P_l = 1.1547$ rule with the smaller fin pitch in Figs. 14(a) and 14(b) has a similar smooth velocity and temperature field with only one primary flow in the middle of the channel. This is similar to the best design without restrictions in Figs. 10(b) and 10(c). The best performing design that follows $P_t/P_l = 1.1547$ rule with the larger fin pitch in Figs. 14(c) and 14(d) in contrast has a much narrower flow path and the re-circulation zone extends much further downstream when compared to all the other best performing designs.

In a situation where the $P_t/P_l = 1.1547$ tube pattern rule is followed, the tube pattern with highest performance ratio with the smaller fin pitch $F_p = 1.5$ mm has a 61% higher JF performance ratio than with the larger fin pitch of $F_p = 3.5$ mm. The observation can be largely explained by a 5.7% reduction in j-factor and 34.4% reduction in friction factor. This is consistent with the literature although such absolute comparison has not been made before for a specific application that has a collection of design restrictions. We assume that these findings can be reproduced for each tube size independently. Only then, a comprehensive comparison can be made between the best performing tube pattern of each tube size, inlet velocity and fin pitch combination. This would enable the manufacturers of the heat exchangers to make a direct comparison between the benefits gained from only changing the tube pattern and changing both the tube size and the tube pattern.

From all the numerical data in this study, a conclusion can be made that the maximum possible performance ratio JF for plain fins with a tube diameter of $D_c = 10.00$ mm is not found in the area of the current portfolio that is manufactured in the industry and the experimental data available in the literature. Therefore, it is possible that the correlation equations that are used in the industry and are made based on the experimental data, cannot predict the performance of unorthodox tube patterns correctly. This means that by performing an optimization study based on the correlation equations, as is commonly done in the industry, it is unlikely to find the same optimal tube patterns that were shown in this study. As the amount of CFD results in the literature is increasing with a rapid pace, a similar correlation study should be performed and correlation equations should be made for computational results. This study contributes a comprehensive and systematic collection of 198 data points for the specific part of the design space with one inlet velocity of $u = 3\,\mathrm{m\,s^{-1}}$, two different fin pitches $F_p = 1.5$ mm and $F_p = 3.5$ mm, number of tube rows $N = 4$, tube diameter $D = 10.00$ mm, the fin thickness $t = 0.2$ mm and the range of longitudinal tube pitch $P_l = 14{-}78$ mm and transverse tube pitch $P_t = 14{-}38$ mm.

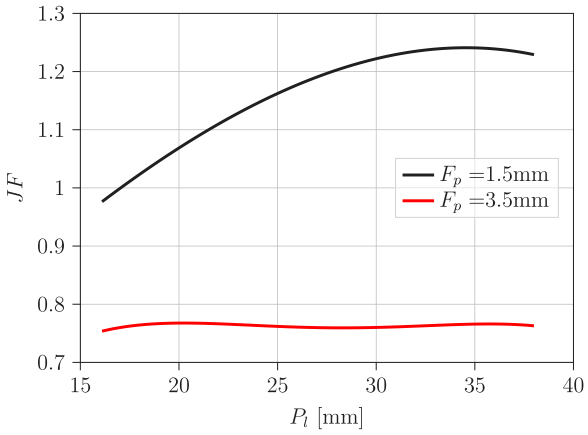

Fig. 13. JF performance ratio regression model for following the $P_t/P_l = 1.1547$ ratio.

5. Conclusions

In this study, we investigated the optimal tube arrangements for a fin-and-tube (FTHE) heat exchanger with plain fins for two application-specific fin pitches $F_p = 1.5$ mm and 3.5 mm. The smaller fin pitch represents a FTHE design for dry filtered air. In contrast, the larger fin pitch represents a typical design with high condensation rate and unfiltered air. Both cases are relevant to marine HVAC applications with a typical design inlet velocity of $u = 3\,\mathrm{m\,s^{-1}}$. The thermal-hydraulic efficiency of the FTHE design was measured by comparing the JF performance ratio of each design. The selection of different tube patterns covered longitudinal tube pitch $P_l = 14{-}78$ mm and transverse tube pitch $P_t = 14{-}38$ mm, resulting in 198 simulated designs. From this, the following conclusions are made:

1. If application-specific additional constraints, related to air with high humidity or impurities, are not applied, the smaller fin pitch $F_p = 1.5$ mm may offer 36% better JF performance ratio than the design $F_p = 3.5$ mm.
2. For unconstrained tube arrangements, the local maximum performance ratio of $JF = 1.28$ for the fin pitch $F_p = 1.5$ mm is found and for the fin pitch $F_p = 3.5$ mm the maximum performance ratio of $JF = 0.94$ can be achieved.
3. For constrained tube arrangements, $P_t/P_l = 1.1547$, the local maximum of the performance ratio is $JF = 1.24$ for the fin pitch $F_p = 1.5$ mm and for the fin pitch $F_p = 3.5$ mm the maximum performance ratio of $JF = 0.77$ can be achieved.
4. Thus, by neglecting the manufacturing restrictions related to the radius of the hairpins in the soldering process of the tube circuits, a 4% higher JF performance ratio for fin pitch $F_p = 1.5$ mm and 23% higher JF performance ratio for fin pitch $F_p = 3.5$ mm can be achieved.
5. The results indicate that unconventional tube arrangement ratio values $P_t/P_l \neq 1.1547$ may offer better performance with regard to the JF performance ratio. We propose that such values should be considered in future FTHE designs.

Regarding all the numerical data in this study, a conclusion can be made that the maximum possible performance ratio JF for plain fins with a tube diameter of $D_c = 10.00$ mm is not found in the area of the current portfolio that is manufactured in the industry. Based on the computational results presented in this study, the new tube patterns should be manufactured, measured and new improved correlation equations should be created for the industry. This could enable the industry to manufacture better performing application specific heat exchangers in the future. The results are shared as a comma-separated value (csv) file. The data should be used as a part of a data bank

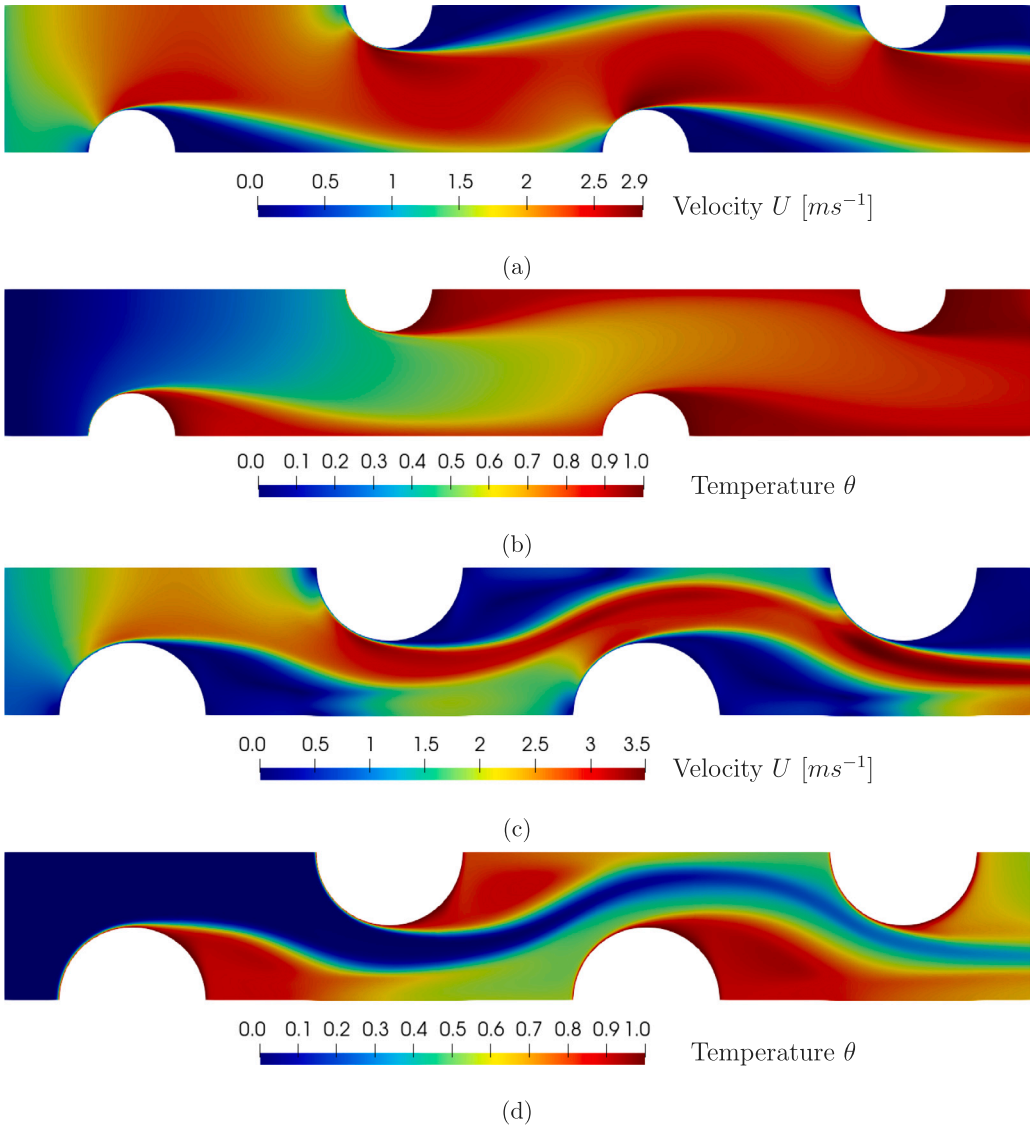

Fig. 14. (a) Velocity in the middle of the channel with F_p = 1.5 mm, P_l = 29.79 mm and P_t = 34.26 mm (b) Temperature in the middle of the channel with F_p = 1.5 mm, P_l = 29.79 mm and P_t = 34.26 mm (c) Velocity in the middle of the channel with F_p = 3.5 mm, P_l = 17.58 mm and P_t = 20.22 mm (d) Temperature in the middle of the channel with F_p = 3.5 mm, P_l = 17.58 mm and P_t = 20.22 mm.

Table 3
Coefficients and the quality indicators of the regression models.

Responses	F_p = 1.5 mm		F_p = 3.5 mm	
	Coefficient	Std err	Coefficient	Std err
b_0	0.48	0.42	−0.32	0.26
b_1	−23.69	11.10	23.19	6.98
b_2	55.12	64.87	188.13	40.79
b_{11}	−659.77	275.31	78.34	173.13
b_{12}	−6798.87	767.68	3307.57	482.75
b_{22}	−5540.69	3828.94	1240.29	2497.83
b_{111}	17077.78	3665.94	997.29	2305.33
b_{112}	72750.02	7884.42	−26166.21	4958.12
b_{122}	−125539.79	23545.95	−62106.19	14806.86
b_{222}	147477.31	99063.08	303669.22	62295.79
b_{1111}	−104797.69	19160.09	−6732.87	12048.82
b_{1112}	294342.54	40918.26	66435.03	25731.43
b_{1122}	529892.66	10540.53	261357.07	66284.12
b_{1222}	816672.01	275148.25	338885.09	173026.90
b_{2222}	1281645.61	944518.36	−2583721.16	593960.10
R^2	0.967		0.985	
Pred. R^2	0.942		0.979	

for generating more accurate surrogate models for the industry of manufacturing fin-and-tube heat exchangers.

Declaration of competing interest

The authors declare that they have no known competing financial interests or personal relationships that could have appeared to influence the work reported in this paper.

Acknowledgment

The authors wish to acknowledge CSC – IT Center for Science, Finland, for computational resources and Koja Oy, for financial support.

Appendix

See Tables 2 and 3.

References

[1] T. Cao, H. Lee, Y. Hwang, R. Radermacher, H.-H. Chun, Performance investigation of engine waste heat powered absorption cycle cooling system for shipboard applications, Appl. Therm. Eng. (ISSN: 1359-4311) 90 (2015) 820–830, http://dx.doi.org/10.1016/j.applthermaleng.2015.07.070, URL http://www.sciencedirect.com/science/article/pii/S135943111500767X.

[2] F. Baldi, F. Ahlgren, T.-V. Nguyen, M. Thern, K. Andersson, Energy and exergy analysis of a cruise ship, Energies 11 (10) (2018) 2508.

[3] G. Barone, A. Buonomano, C. Forzano, A. Palombo, M. Vicidomini, Sustainable energy design of cruise ships through dynamic simulations: Multi-objective optimization for waste heat recovery, Energy Convers. Manage. (ISSN: 0196-8904) 221 (2020) 113166, http://dx.doi.org/10.1016/j.enconman.2020.113166, URL http://www.sciencedirect.com/science/article/pii/S019689042030710X.

[4] G. Xie, Q. Wang, B. Sunden, Parametric study and multiple correlations on air-side heat transfer and friction characteristics of fin-and-tube heat exchangers with large number of large-diameter tube rows, Appl. Therm. Eng. (ISSN: 1359-4311) 29 (1) (2009) 1–16, http://dx.doi.org/10.1016/j.applthermaleng.2008.01.014, URL https://www.sciencedirect.com/science/article/pii/S135943110800029X.

[5] R. Borrajo-Pelaez, J. Ortega-Casanova, J. Cejudo-Lopez, A three-dimensional numerical study and comparison between the air side model and the air/water side model of a plain fin-and-tube heat exchanger, Appl. Therm. Eng. (ISSN: 1359-4311) 30 (13) (2010) 1608–1615, http://dx.doi.org/10.1016/j.applthermaleng.2010.03.018, URL https://www.sciencedirect.com/science/article/pii/S1359431110001286.

[6] C.-T. Hsieh, J.-Y. Jang, Parametric study and optimization of louver finned-tube heat exchangers by taguchi method, Appl. Therm. Eng. (ISSN: 1359-4311) 42 (2012) 101–110, http://dx.doi.org/10.1016/j.applthermaleng.2012.03.003, Heat Powered Cycles Conference, 2009. URL https://www.sciencedirect.com/science/article/pii/S1359431112001585.

[7] A.A. Bhuiyan, M.R. Amin, A.S. Islam, Three-dimensional performance analysis of plain fin tube heat exchangers in transitional regime, Appl. Therm. Eng. (ISSN: 1359-4311) 50 (1) (2013) 445–454, http://dx.doi.org/10.1016/j.applthermaleng.2012.07.034, URL https://www.sciencedirect.com/science/article/pii/S1359431112005169.

[8] R. Yun, Y. Kim, Y. Kim, Air side heat transfer characteristics of plate finned tube heat exchangers with slit fin configuration under wet conditions, Appl. Therm. Eng. (ISSN: 1359-4311) 29 (14) (2009) 3014–3020, http://dx.doi.org/10.1016/j.applthermaleng.2009.03.017, URL https://www.sciencedirect.com/science/article/pii/S1359431109000994.

[9] W. Ding, J. Fan, Y. He, W. Tao, Y. Zheng, Y. Gao, J. Song, A general simulation model for performance prediction of plate fin-and-tube heat exchanger with complex circuit configuration, Appl. Therm. Eng. (ISSN: 1359-4311) 31 (16) (2011) 3106–3116, http://dx.doi.org/10.1016/j.applthermaleng.2011.01.045, URL https://www.sciencedirect.com/science/article/pii/S1359431111000706.

[10] J. Wu, W. Tao, Investigation on laminar convection heat transfer in fin-and-tube heat exchanger in aligned arrangement with longitudinal vortex generator from the viewpoint of field synergy principle, Appl. Therm. Eng. (ISSN: 1359-4311) 27 (14) (2007) 2609–2617, http://dx.doi.org/10.1016/j.applthermaleng.2007.01.025, URL https://www.sciencedirect.com/science/article/pii/S1359431107000488.

[11] M. Li, H. Zhang, J. Zhang, Y. Mu, E. Tian, D. Dan, X. Zhang, W. Tao, Experimental and numerical study and comparison of performance for wavy fin and a plain fin with radiantly arranged winglets around each tube in fin-and-tube heat exchangers, Appl. Therm. Eng. (ISSN: 1359-4311) 133 (2018) 298–307, http://dx.doi.org/10.1016/j.applthermaleng.2018.01.012.

[12] C.-C. Wang, K.-Y. Chi, C.-J. Chang, Heat transfer and friction characteristics of plain fin-and-tube heat exchangers, part II: Correlation, Int. J. Heat Mass Transfer (ISSN: 0017-9310) 43 (15) (2000) 2693–2700, http://dx.doi.org/10.1016/S0017-9310(99)00333-6.

[13] C.-C. Wang, K.-Y. Chi, C.-J. Chang, Heat transfer and friction characteristics of plain fin-and-tube heat exchangers, part II: Correlation, Int. J. Heat Mass Transfer 43 (15) (2000) 2693–2700.

[14] C.-C. Wang, Y.-J. Chang, Y.-C. Hsieh, Y.-T. Lin, Sensible heat and friction characteristics of plate fin-and-tube heat exchangers having plane fins, Int. J. Refrig. 19 (4) (1996) 223–230.

[15] C.-C. Wang, Y.-M. Hwang, Y.-T. Lin, Empirical correlations for heat transfer and flow friction characteristics of herringbone wavy fin-and-tube heat exchangers, Int. J. Refrig. 25 (5) (2002) 673–680.

[16] C.-C. Wang, W.-S. Lee, W.-J. Sheu, A comparative study of compact enhanced fin-and-tube heat exchangers, Int. J. Heat Mass Transfer 44 (18) (2001) 3565–3573.

[17] B. Ameel, J. Degroote, H. Huisseune, J. Vierendeels, M.D. Paepe, Interaction effects between parameters in a vortex generator and louvered fin compact heat exchanger, Int. J. Heat Mass Transfer (ISSN: 0017-9310) 77 (2014) 247–256, http://dx.doi.org/10.1016/j.ijheatmasstransfer.2014.04.073, URL http://www.sciencedirect.com/science/article/pii/S0017931014003913.

[18] C.-C. Wang, Y.-J. Du, Y.-J. Chang, W.-H. Tao, Airside performance of herringbone fin-and-tube heat exchangers in wet conditions, Can. J. Chem. Eng. 77 (6) (1999) 1225–1230.

[19] J.A. Siegel, W.W. Nazaroff, Predicting particle deposition on HVAC heat exchangers, Atmos. Environ. (ISSN: 1352-2310) 37 (39) (2003) 5587–5596, http://dx.doi.org/10.1016/j.atmosenv.2003.09.033, Indoor Air Chemistry and Physics: Papers from Indoor Air 2002.

[20] Y. Xia, Y. Zhong, P. Hrnjak, A. Jacobi, Frost, defrost, and refrost and its impact on the air-side thermal-hydraulic performance of louvered-fin, flat-tube heat exchangers, Int. J. Refrig. (ISSN: 0140-7007) 29 (7) (2006) 1066–1079, http://dx.doi.org/10.1016/j.ijrefrig.2006.03.005, URL http://www.sciencedirect.com/science/article/pii/S0140700706000648.

[21] C.-C. Wang, C.-J. Lee, C.-T. Chang, Y.-J. Chang, Some aspects of plate fin-and-tube heat exchangers: with and without louvers, J. Enhanc. Heat Transf. 6 (5) (1999).

[22] C.-C. Wang, J.-Y. Chang, N.-F. Chiou, Effects of waffle height on the air-side performance of wavy fin-and-tube heat exchangers, Heat Transf. Eng. 20 (3) (1999) 45–56.

[23] D.G. Rich, The effect of fin spacing on the heat transfer and friction performance of multi-row, smooth plate fin-and-tube heat exchangers, AsHRAE Trans. 79 (2) (1973) 135–145.

[24] D.G. Rich, The effect of the number of tube rows on heat transfer performance of smooth plate fin-and-tube heat exchangers, 1975, Unknown.

[25] Y. Seshimo, M. Fujii, An experimental study on the performance of plate fin and tube heat exchangers at low Reynolds numbers, in: Proceedings of the 1991 ASME JSME Thermal Engineering Joint Conference, 1991, pp. 673–680.

[26] M.-Y. Wen, C.-Y. Ho, Heat-transfer enhancement in fin-and-tube heat exchanger with improved fin design, Appl. Therm. Eng. (ISSN: 1359-4311) 29 (5) (2009) 1050–1057, http://dx.doi.org/10.1016/j.applthermaleng.2008.05.019, URL https://www.sciencedirect.com/science/article/pii/S1359431108002457.

[27] C.-C. Wang, Y.-J. Chang, Y.-C. Hsieh, Y.-T. Lin, Sensible heat and friction characteristics of plate fin-and-tube heat exchangers having plane fins, Int. J. Refrig. 19 (4) (1996) 223–230.

[28] C. Luo, S. Wu, K. Song, L. Hua, L. Wang, Thermo-hydraulic performance optimization of wavy fin heat exchanger by combining delta winglet vortex generators, Appl. Therm. Eng. (ISSN: 1359-4311) 163 (2019) 114343, http://dx.doi.org/10.1016/j.applthermaleng.2019.114343, URL https://www.sciencedirect.com/science/article/pii/S1359431119322781.

[29] G. C., Transport Processes and Separation Process Principles (Includes Unit Operations), Prentice Hall Press, 2003.

[30] W.M. Kays, A.L. London, Compact Heat Exchangers, Vol. 196, McGraw-Hill New York, 1958.

[31] R.L. Webb, N. Kim, Enhanced Heat Transfer, Taylor and Francis, NY, 2005.

[32] A. London, C. Ferguson, Test results of high-performance heat exchanger surfaces used in aircraft intercoolers and their significance for gas-turbine regenerator design, Trans. ASME 71 (1949) 17–26.

[33] R.K. Shah, A.L. London, Flow Forced Convection Heat Transfer and Flow Friction in Straight and Curved Ducts - A Summary of Analytical Solutions, Vol. 1, No. 1, Academic Press, ISBN: 1483191303, 1972, p. 311.

[34] K. Stone, Review of Literature on Heat Transfer Enhancement in Compact Heat Exchangers, Tech. Rep., Air Conditioning and Refrigeration Center. College of Engineering, 1996.

[35] B. Shi, L. Wang, F. Gen, Y. Zhang, The optimal fin spacing for three-row flat tube bank fin mounted with vortex generators, Heat Mass Transf. 43 (1) (2006) 91–101.

[36] J.-Y. Yun, K.-S. Lee, Influence of design parameters on the heat transfer and flow friction characteristics of the heat exchanger with slit fins, Int. J. Heat Mass Transfer 43 (14) (2000) 2529–2539.

[37] L.O. Salviano, D.J. Dezan, J.I. Yanagihara, Optimization of winglet-type vortex generator positions and angles in plate-fin compact heat exchanger: Response Surface Methodology and Direct Optimization, Int. J. Heat Mass Transfer (ISSN: 0017-9310) 82 (2015) 373–387, http://dx.doi.org/10.1016/j.ijheatmasstransfer.2014.10.072, URL https://www.sciencedirect.com/science/article/pii/S0017931014009727.

[38] L.O. Salviano, D.J. Dezan, J.I. Yanagihara, Thermal-hydraulic performance optimization of inline and staggered fin-tube compact heat exchangers applying longitudinal vortex generators, Appl. Therm. Eng. (ISSN: 1359-4311) 95 (2016) 311–329, http://dx.doi.org/10.1016/j.applthermaleng.2015.11.069, URL https://www.sciencedirect.com/science/article/pii/S1359431115013150.

[39] M.F. Md Salleh, H.A. Mohammed, M.A. Wahid, Thermal and hydraulic characteristics of trapezoidal winglet across fin-and-tube heat exchanger (FTHE), Appl. Therm. Eng. (ISSN: 1359-4311) 149 (2019) 1379–1393, http://dx.doi.org/10.1016/j.applthermaleng.2018.12.098, URL https://www.sciencedirect.com/science/article/pii/S1359431118358034.

[40] FOAM-extend, FOAM-extend, 2017, URL http://foam-extend.org/.

[41] T. Välikangas, R. Karvinen, Conjugated heat transfer simulation of a fin-and-tube heat exchanger, Heat Transf. Eng. 39 (13–14) (2018) 1192–1200.

[42] T. Välikangas, S. Singh, K. Sørensen, T. Condra, Fin-and-tube heat exchanger enhancement with a combined herringbone and vortex generator design, Int. J. Heat Mass Transfer (ISSN: 0017-9310) 118 (2018) 602–616, http://dx.doi.org/10.1016/j.ijheatmasstransfer.2017.11.006.

[43] T. Välikangas, J. Hærvig, H. Kuuluvainen, M.D. Maso, P. Peltonen, V. Vuorinen, Deposition of dry particles on a fin-and-tube heat exchanger by a coupled soft-sphere DEM and CFD, Int. J. Heat Mass Transfer (ISSN: 0017-9310) 149 (2020) 119046, http://dx.doi.org/10.1016/j.ijheatmasstransfer.2019.119046.

[44] T.L. Bergman, F.P. Incropera, D.P. DeWitt, A.S. Lavine, Fundamentals of Heat and Mass Transfer, John Wiley & Sons, 2011.

[45] S. Patankar, C. Liu, E.M. Sparrow, Fully developed flow and heat transfer in ducts having streamwise-periodic variations of cross-sectional area, J. Heat Transfer (1977).

[46] C.T. Lawrence, A.L. Tits, A computationally efficient feasible sequential quadratic programming algorithm, SIAM J. Optim. 11 (4) (2001) 1092–1118.